Method to measure efficiently rare fluctuations of turbulence intensity for turbulent-laminar transitions in pipe flows

Takahiro Nemoto[1] and Alexandros Alexakis[2]

[1]*Philippe Meyer Institute for Theoretical Physics, Physics Department, École Normale Supérieure & PSL Research University, 24 rue Lhomond, 75231 Paris Cedex 05, France*
[2]*Laboratoire de Physique Statistique, École Normale Supérieure, CNRS, Université Pierre et Marié Curie, Université Paris Diderot, 24 rue Lhomond, 75005 Paris Cedex 05, France*

The fluctuations of turbulence intensity in a pipe flow around the critical Reynolds number is difficult to study but important because they are related to turbulent-laminar transitions. We here propose a rare-event sampling method to study such fluctuations in order to measure the time scale of the transition efficiently. The method is composed of two parts: (i) the measurement of typical fluctuations (the bulk part of an accumulative probability function) and (ii) the measurement of rare fluctuations (the tail part of the probability function) by employing dynamics where a feedback control of the Reynolds number is implemented. We apply this method to a chaotic model of turbulent puffs proposed by Barkley and confirm that the time scale of turbulence decay increases super exponentially even for high Reynolds numbers up to Re = 2500, where getting enough statistics by brute-force calculations is difficult. The method uses a simple procedure of changing Reynolds number that can be applied even to experiments.

I. INTRODUCTION

In 1883, Reynolds used a dimensionless quantity to characterize pipe flows, the well-known Reynolds number Re [1]. This number, defined from the velocity, density, pipe diameter, and the viscosity of fluid, determines the pattern of flows: the flows tend to be laminar when this number is small and tend to be turbulent when it is large. Reynolds himself believed that there is a transition value Re_c, the so-called critical Reynolds number, that distinguishes these two patterns of flows. After his proposition, however, many experiments and numerical simulations revealed that the problem was more complex than expected [2–4]. First of all, linear stability analysis shows that the laminar flows are stable for any Reynolds number if the perturbation added to the pipe is infinitesimally small. This means that, in an experiment to observe the transition without adding any perturbation to the pipe, the transition Reynolds number depends on background fluctuations, i.e., it depends on the detailed setting of the experiment. Second, even with a sufficiently strong perturbation to create tiny patches of turbulence (e.g., higher vorticity region) known as puffs [5], these puffs show sudden decaying or splitting into two, whose time scales are extremely long [3,6,7]. Because of this, determining the precise value at which the puffs start to sustain was for a long time an unsolvable task.

A breakthrough came after the detailed studies of puffs that revealed that the time scales of the splitting and decaying are stochastically and independently determined [8–12]. As the Reynolds number increases, the time scale of decaying (or splitting) increases (or decreases). There is thus a special Reynolds number, Re_c, in which these two time scales become equal, and below this value the decaying of puffs is dominant, but above it the splitting of puffs is dominant. In 2011,

more than a century after Reynolds's proposition, Avila *et al.* measured Re_c by studying these two time scales of puffs [13] finding a transition Reynolds number Re_c around Re = 2040. The obstacle of this measurement was that these time scales became extremely long when Re was close to Re_c. Avila *et al.* overcame this difficulty by preparing a long (15 m) pipe, but in their paper, they also stated that they could not observe the puff decaying and splitting within numerical simulations for Re ∼ Re_c, due to high computational costs.

The study of the turbulent-laminar transition is difficult around Re_c, because the puffs are weakly unstable [14], and splitting and decaying are observed as rare events. In fact a superexponential increase of the puff-decaying time scale has been observed as a function of the Reynolds number [8,9] and its origin has been discussed using the extreme value statistics [15–18] and directed percolation models [19,20], but it is still unclear if this is an effective law observed only around Re_c or if it can be observed beyond. The goal of this paper is to introduce a sampling method to help this situation by accelerating the measurement of the puff decaying. For the application of this method, we use a coupled map lattice model [21] to describe the puff dynamics that has been proposed by Barkley [22] (below we call it the Barkley model). However, we stress that our method can be applied to more realistic systems, including DNS of Navier-Stokes equation and experiments.

The structure of this paper is as follows. We first discuss the relation between the puff-decaying time scale and a rare-event probability (the tail of an accumulative probability function) in Sec. II. We then introduce the sampling method that uses a feedback control of the Reynolds number in Sec. III. In Sec. IV, we demonstrate the application of the method to the Barkley model, and we show that the superexponential increase of the puff-decaying time scale is observed up to Re = 2500. Within
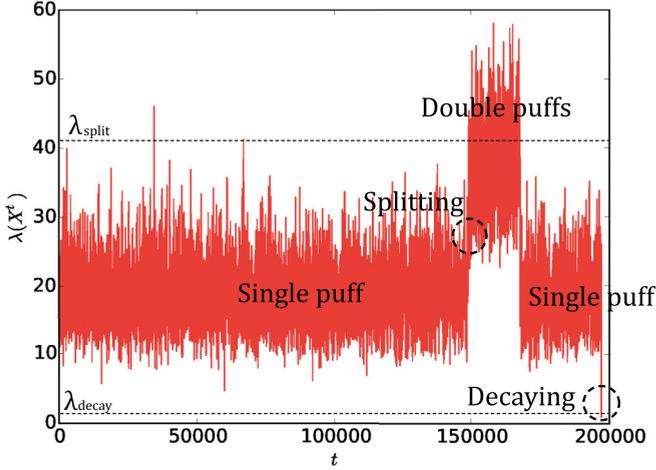
FIG. 1. Typical time-series data of the total turbulence intensity $\lambda(X)$ in the Barkley model [22] with Re = 2046, showing puff splitting and puff decaying. When there is only a single puff, $\lambda(X)$ takes a value from 10 to 30 (approximately), but when there are two puffs, it takes a value from 30 to 60. Furthermore, as the puff decays, $\lambda(X)$ converges to 0. We thus define threshold values of λ to judge if there exists only one puff in our pipe as $\lambda_{\mathrm{decay}} = 1$ and $\lambda_{\mathrm{split}} = 41$, which are used throughout this paper [23]. Note that, although we show a decay of puff from a double-puff state to a single-puff state around $t = 1.7 \times 10^5$ in this figure, our measurement of puff-decaying time scale described in Sec. II takes into account only the decay from a single-puff state.

this section, we also discuss the improvement of calculation efficiency of the method (Sec. IV D). In Sec. V, we conclude this paper. We note that the detailed definition of the Barkley model is provided in Appendix A.

II. FLUCTUATIONS AND PUFF-DECAYING TIME SCALE

We first discuss the connection between the fluctuations of the turbulence intensity and the time scale of puff decaying. Let us consider a pipe flow, where we denote the velocity field of the flow by X (also by X^t the field X at time t). The total turbulence intensity is calculated from the field X (e.g., by the total energy in the radial component of X or by the axial component of average vorticity), which we denote by $\lambda(X)$. For the Barkley model (whose definition is shown in Appendix A), typical dynamics of $\lambda(X)$ is presented in Fig. 1. One can see that $\lambda(X)$ is fluctuating around a certain value, and $\lambda(X)$ becomes twice as big as this certain value when the puff is split into two while it takes almost 0 after the puff decays. In order to define relaminalized (puff-decayed) states quantitatively, we introduce a threshold value λ_{decay}, such that the puff almost certainly decays once $\lambda(X)$ takes a value smaller than λ_{decay}. Furthermore, in order to focus on decay events from a single-puff state, we introduce another threshold value λ_{split} that distinguishes these two puff states (Fig. 1). By using these two threshold values, we consider the following measurement of the time scale of puff decaying from a single-puff state.

(i) We start a simulation (or an experiment) to observe the turbulent puff by adding a localized perturbation to laminar flows (where only a single small puff is created). After an initial

relaxation time τ_{ini}, we check that the puff satisfies $\lambda_{\mathrm{decay}} < \lambda(X^t) < \lambda_{\mathrm{split}}$ with $t = \tau_{\mathrm{ini}}$. We repeat (i) until we get a state that satisfies this inequality.

(ii) During the time evolution of the puff ($t \geqslant \tau_{\mathrm{ini}}$), we store the value of $\lambda(X^t)$ for each time interval δt_m. We stop this simulation when $\lambda_{\mathrm{decay}} < \lambda(X^t) < \lambda_{\mathrm{split}}$ is violated. [More precisely, we stop the simulation the first time we store $\lambda(X^t)$ after $\lambda_{\mathrm{decay}} \geqslant \lambda(X^t)$ or $\lambda(X^t) \leqslant \lambda_{\mathrm{split}}$ holds.]

(iii) When we stop the simulation, if $\lambda_{\mathrm{decay}} \geqslant \lambda(X^t)$, we increment a number n_{decay} (which starts at 0 at the beginning of the entire measurements) by 1. We also increment the total number of measurements n_{tot} (which also starts at 0 at the beginning of the entire measurements) by $(t - \tau_{\mathrm{ini}})/\delta t_m$, where t is the time when $\lambda_{\mathrm{decay}} < \lambda(X^t) < \lambda_{\mathrm{split}}$ becomes violated.

After repeating this measurement many times, we get the estimate of the decaying time scale T_{d} as

$$T_{\mathrm{d}} = \frac{n_{\mathrm{tot}} \delta t_m}{n_{\mathrm{decay}}}. \tag{1}$$

In Refs. [8,9,22], the puff-decaying time scale is measured from an exponential fitting to the probability distribution function of (each) puff-decaying time. Different from their measurements, our estimator (1) directly gives the expected value of the puff-decaying time. (Our estimator is equivalent to the one used in Refs. [8,9,22] when n_{decay} is sufficiently large.) In many experiments and numerical simulations, it has been observed that T_{d} scales in a superexponential way as a function of Re [8,9], i.e., a measurement of T_{d} based on brute-force calculations becomes harder as the Reynolds number increases.

T_{d} is connected to rare fluctuations of the turbulence intensity. To see this, we define an accumulative probability function of $\lambda(X)$ as follows: by denoting the obtained (total) time series of λ by λ^i ($i = 1, 2, \ldots, n_{\mathrm{tot}}$), we define

$$P(\lambda) = \frac{1}{n_{\mathrm{tot}}} \sum_{i=1}^{n_{\mathrm{tot}}} \theta(\lambda - \lambda^i), \tag{2}$$

where $\theta(\lambda)$ is the Heaviside step function: $\theta(\lambda) = 1$ for $\lambda > 0$ and $\theta(\lambda) = 0$ for $\lambda \leqslant 0$. By definition, we have $P(\lambda_{\mathrm{decay}}) = n_{\mathrm{decay}}/n_{\mathrm{tot}}$. From (1), we find

$$P(\lambda_{\mathrm{decay}}) = \frac{\delta t_{\mathrm{m}}}{T_{\mathrm{d}}}, \tag{3}$$

namely, the tail value of the accumulative probability $P(\lambda)$ is connected to the inverse of the puff-decaying time scale.

III. REYNOLDS-NUMBER-CONTROLLED PROCEDURE

To measure the tail of $P(\lambda)$ efficiently, we propose a simple procedure to control the Reynolds number during the measurement. In Fig. 2, we show numerical examples of $P(\lambda)$ in the Barkley model [22] for several Reynolds numbers. One can see that the domain of this probability function is separated into two parts: large-λ part and small-λ part. The large-λ part is described by the typical dynamics, whereas the small-λ part is described by the dynamics of atypically small puffs. In the small-λ part, the slope of $P(\lambda)$ (in logarithmic scale) is smaller than the one in the large-λ part. This observation suggests the existence of a relatively stable state for small puffs before decaying, which we call the metastable state in this paper. What
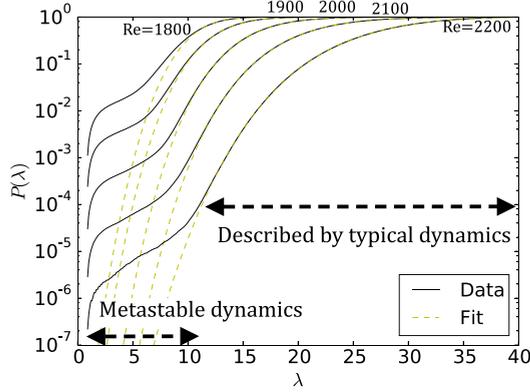
FIG. 2. The accumulative probability function $P(\lambda)$ for several Reynolds numbers in the Barkley model [22] obtained from brute-force measurements. $P(\lambda)$ shows two different behaviors, namely (i) the one described by typical dynamics of the puffs and (ii) the one described by relatively stable dynamics (metastable dynamics) before the puffs decay. For the typical part, we fit to the data a superexponential function defined as (15), which shows good agreement with the typical part of $P(\lambda)$.

we propose is a procedure to change the Reynolds number to efficiently create such a metastable state.

Let us suppose that we want to study the tail of $P(\lambda)$ at $\mathrm{Re} = \mathrm{Re}_1$. We define another Reynolds number Re_0 that is smaller than Re_1 ($\mathrm{Re}_0 < \mathrm{Re}_1$), where a puff tends to become small easily. We also define two special values of the turbulence intensity, λ_0 and λ_1 ($\lambda_0 \geqslant \lambda_1$), at which we switch the Reynolds number. More precisely, during the procedures (i) and (ii) explained in the previous section, the following control of the Reynolds number (Re-control) is performed: we set the Reynolds number to Re_1 when $\lambda(X^t)$ crosses λ_1 and to Re_0 when $\lambda(X^t)$ crosses λ_0. We show a schematic figure to explain this control in Fig. 3. After finishing this procedure, we collect the time-series data of $\lambda(X)$ (in the same way as the brute-force method) and calculate the accumulative probability function of λ, which we denote by $P_{\mathrm{tail}}(\lambda)$. What we expect is that this functional shape of $P_{\mathrm{tail}}(\lambda)$ can provide a good approximation
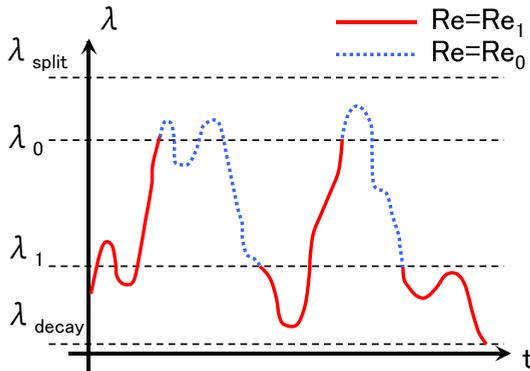

FIG. 3. Schematic figure to explain the procedure to control the Reynolds number (Re-control) during the measurement. When λ crosses λ_1 (or λ_0), we change the Reynolds number to Re_1 (or to Re_0), where $\mathrm{Re}_1 > \mathrm{Re}_0$ and $\lambda_1 < \lambda_0$. The accumulative probability of λ in this procedure is our estimator for the tail of $P(\lambda)$.

of the correct probability $P(\lambda)$ for small λ [tail of $P(\lambda)$]. More precisely, we expect $P(\lambda) \simeq C P_{\mathrm{tail}}(\lambda)$ for $\lambda \lesssim \lambda^*$ with two constants C and λ^*, which are determined by the following conditions:

$$C P_{\mathrm{tail}}(\lambda^*) = P(\lambda^*), \tag{4}$$

$$C \frac{d P_{\mathrm{tail}}(\lambda^*)}{d\lambda} = \frac{d P(\lambda^*)}{d\lambda}. \tag{5}$$

After determining these constants, our estimator of $P(\lambda)$ is

$$P(\lambda) \simeq \begin{cases} C P_{\mathrm{tail}}(\lambda) & \text{for } \lambda < \lambda^* \\ P(\lambda) & \text{for } \lambda \geqslant \lambda^*. \end{cases} \tag{6}$$

Note that obtaining $P(\lambda)$ for $\lambda \geqslant \lambda^*$ is easier than obtaining the full shape of $P(\lambda)$ from brute-force calculations. Finally, we obtain the estimator of the decaying time scale T_{d} in our method as

$$T_{\mathrm{d}} \simeq \frac{\delta t_m}{C P_{\mathrm{tail}}(\lambda_{\mathrm{decay}})} \tag{7}$$

from (3).

IV. APPLICATION TO BARKLEY MODEL

In this section, we apply Re-control method to a model of puff dynamics proposed by Barkley [22]. To this end, in Sec. IV A, we first discuss how to choose three parameters λ_0, λ_1, and Re_0 appearing in the method. The criteria to choose them are also summarized in Table I. We then show the results of the application in Sec. IV B, followed by the discussion on how much the method accelerates the measurement of the time scale T_d in Sec. IV D.

A. Parameters λ_0, λ_1, and Re_0
1. Criterion for λ_0

In the method, the Reynolds number is set to a smaller value Re_0 from the target Reynolds number Re_1 at $\lambda = \lambda_0$ in order to suppress the growth of puff and to weaken it. However, if λ_0 is too small, the puff does not have enough time to evolve in the target Reynolds Re_1 and is suppressed before its equilibration. We thus set the value of λ_0 to be equal or larger than the typical value of λ in the target Reynolds number $\mathrm{Re} = \mathrm{Re}_1$. More precisely, by introducing a probability density $p(\lambda)$ as

$$p(\lambda) = \frac{d}{d\lambda} P(\lambda), \tag{8}$$

we denote the average value of λ for the Reynolds number Re by

$$\bar{\lambda}_{\mathrm{Re}} = \int d\lambda \, p(\lambda)\lambda. \tag{9}$$

We then assign a condition to λ_0 as

$$\lambda_0 = \bar{\lambda}_{\mathrm{Re}_1}. \tag{10}$$

Note that although this condition may be weakened as $\lambda_0 \geqslant \bar{\lambda}_{\mathrm{Re}_1}$, we use (10) for the simplicity of the argument. We stress that calculating $\bar{\lambda}_{\mathrm{Re}_1}$ is not difficult, since it does not require the tail values of the probability $P(\lambda)$. Numerical examples of $\bar{\lambda}_{\mathrm{Re}}$ are provided in Table II.

TABLE I. Criteria to choose the parameters λ_0, λ_1, and Re_0.

	Condition
Higher transition value λ_0	$\lambda_0 = \bar{\lambda}_{\mathrm{Re}_1}$ ($\bar{\lambda}_{\mathrm{Re}_1}$ is the average value of λ for Re_1)
Lower transition value λ_1	$\lambda_{\mathrm{ms}}^{\mathrm{Re}_1} \ll \lambda_1 < \lambda_0 - \sqrt{2\sigma_{\mathrm{Re}_1}}$ [$\lambda_{\mathrm{ms}}^{\mathrm{Re}_1}$ is the boundary value between the metastable and typical regions (Fig 2) for $\mathrm{Re} = \mathrm{Re}_1$. σ^{Re_1} is a variance of λ for Re_1]
Smaller Reynolds number Re_0	$\mathrm{Re}_0 > \mathrm{Re}_1 - \delta\mathrm{Re}^*$ ($\delta\mathrm{Re}^*$ is a constant around $200 \sim 300$)

2. Criterion for λ_1

After changing the Reynolds number from Re_1 to Re_0, the puff is weakened and finally reaches a state that takes $\lambda = \lambda_1$. We then change the Reynolds number from Re_0 to Re_1. We expect that the puff quickly forgets how it is prepared and the statistics for $\lambda < \lambda_1$ obtained afterward is equivalent to the brute-force results [in the sense of (6)]. For this, we discuss the lower and upper bounds of the parameter λ_1 as follows.

We first discuss the upper bound. When λ_1 is too large (i.e., too close to λ_0), the puff often goes back to λ_0 before equilibrating. The method is not efficient in this case, since many failed attempts are needed to get an equilibrated puff that can explore $\lambda < \lambda_1$. In order to prevent this, we assign the upper bound of λ_1 as

$$\lambda_1 < \lambda_0 - \sqrt{2\sigma_{\mathrm{Re}_1}}, \tag{11}$$

where σ_{Re} is the variance of λ calculated from the probability distribution $p(\lambda)$ as

$$\sigma_{\mathrm{Re}} = \int d\lambda \, p(\lambda)(\lambda - \bar{\lambda}_{\mathrm{Re}})^2. \tag{12}$$

Numerical examples of σ_{Re} are shown in Table II.

Next, we discuss the lower bound. If the value of λ_1 is in the metastable range of Fig. 2 (i.e., too small), the puff determines to decay from the configuration before equilibrated after Re is changed to Re_1 at $\lambda = \lambda_1$. These artificial decays carry the information of the lower Reynolds number Re_0 and thus bias the obtained statistics. To prevent this, we set the lower bound of λ_1 as

$$\lambda_1 \gg \lambda_{\mathrm{ms}}^{\mathrm{Re}_1}, \tag{13}$$

where $\lambda_{\mathrm{ms}}^{\mathrm{Re}_1}$ is the boundary value between the metastable and typical regions of $P(\lambda)$ for $\mathrm{Re} = \mathrm{Re}_1$. Within brute-force simulations, this value is determined as the maximum value of λ where the superexponential fit [which is (15) in Sec. IV B] cannot describe $P(\lambda)$. Estimating such an exact value is difficult since it requires the information of the metastable part of $P(\lambda)$. Without knowing this metastable part, what we can get is the higher bound of $\lambda_{\mathrm{ms}}^{\mathrm{Re}_1}$, which we denote $\tilde{\lambda}_{\mathrm{ms}}^{\mathrm{Re}_1}$. This

fact is fortunately compatible with the condition (13): we can get a weaker inequality using such a higher bound by simply replacing $\lambda_{\mathrm{ms}}^{\mathrm{Re}_1}$ in (13) by $\tilde{\lambda}_{\mathrm{ms}}^{\mathrm{Re}_1}$, i.e., the practical condition is $\lambda_1 > \tilde{\lambda}_{\mathrm{ms}}^{\mathrm{Re}_1}$. Rough estimations of $\lambda_{\mathrm{ms}}^{\mathrm{Re}_1}$ are provided in Table II.

3. Criterion for Re_0

By choosing λ_0, λ_1 following the conditions (10), (11), and (13) above, we expect that (6) is satisfied if Re_0 is sufficiently close to Re_1, i.e.,

$$\mathrm{Re}_0 > \mathrm{Re}_1 - \delta\mathrm{Re}^* \tag{14}$$

with a constant $\delta\mathrm{Re}^*$. From numerical simulations for a broad range of Re_1, what we observe is that there indeed exists such a threshold value $\delta\mathrm{Re}^*$, which is around $200 \sim 300$ (see Fig. 5 in Sec. IV C for Re_0 dependence of the estimator T_{d}). To derive such a threshold value $\delta\mathrm{Re}^*$ based on a theory seems difficult, which remains as an important open question.

B. Numerical demonstration of (6): Equivalence between $P(\lambda)$ and $C P_{\mathrm{tail}}(\lambda)$

We numerically demonstrate (6). In order to determine the constant C from the two conditions (4) and (5), we use the shape of the typical part of $P(\lambda)$. In order to make sure that we do not use the information of the tail of $P(\lambda)$ (because it is our goal), we use the following function $P_{\mathrm{fit}}(\lambda)$ instead of $P(\lambda)$, which describes only the typical part:

$$P_{\mathrm{fit}}(\lambda) \propto \int_0^\lambda dx \exp[-\tilde{\gamma}(x - \tilde{\lambda}) - e^{-\tilde{\beta}(x-\tilde{\lambda})}], \tag{15}$$

where $\tilde{\gamma}, \tilde{\lambda}, \tilde{\beta}$ are parameters determined by fitting to $P(\lambda)$. [This fitting can be done without knowing the tail of $P(\lambda)$.] Examples of this function for several Reynolds numbers are shown in Fig. 2. Note that the derivative of $P_{\mathrm{fit}}(\lambda)$ has a simpler form, which is studied in Appendix B. To determine the constant C, we first fix λ^* from the following condition

$$\frac{\partial}{\partial\lambda} \log P_{\mathrm{tail}}(\lambda^*) = \frac{\partial}{\partial\lambda} \log P_{\mathrm{fit}}(\lambda^*). \tag{16}$$

TABLE II. Estimated values of $\bar{\lambda}_{\mathrm{Re}_1}, \sqrt{2\sigma_{\mathrm{Re}_1}}$, and $\lambda_{\mathrm{ms}}^{\mathrm{Re}_1}$.

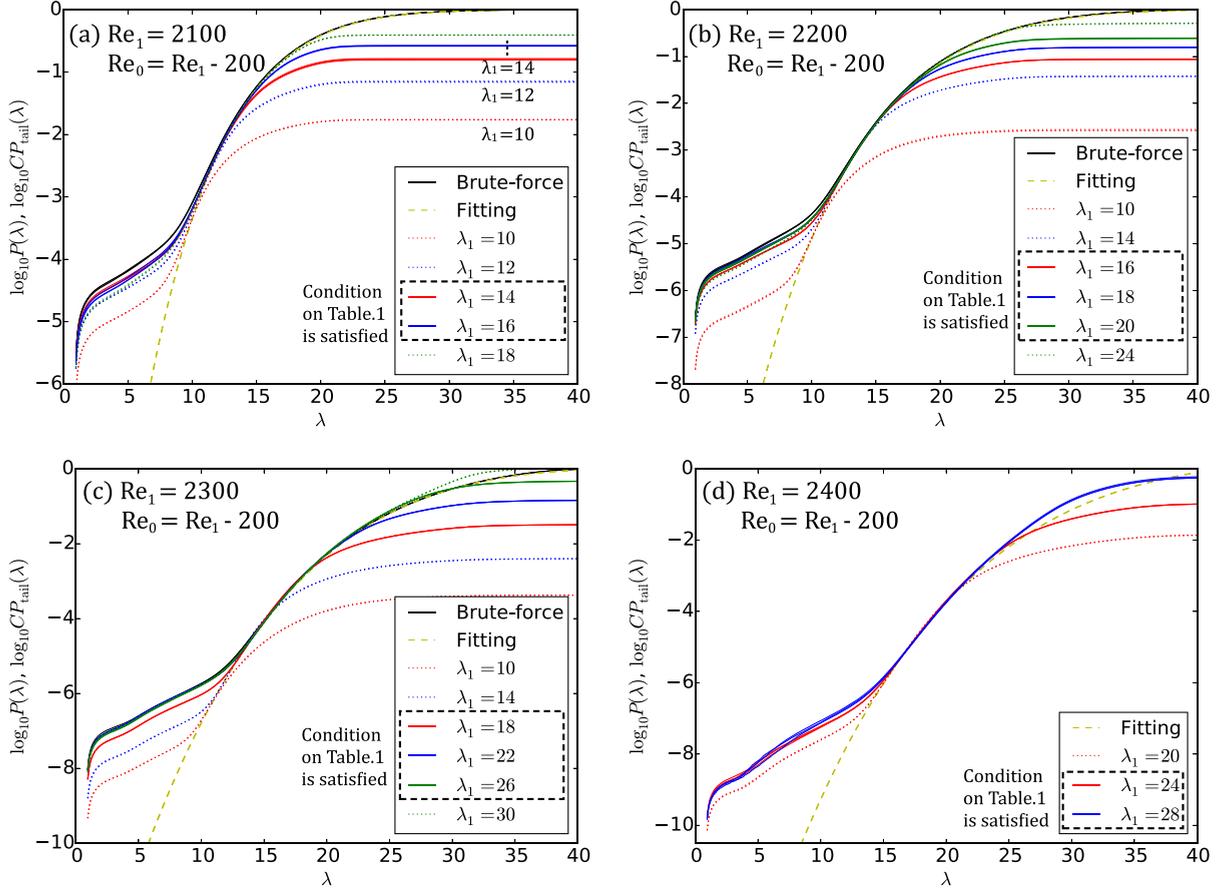|	$\mathrm{Re}_1 = 2100$	$\mathrm{Re}_1 = 2200$	$\mathrm{Re}_1 = 2300$	$\mathrm{Re}_1 = 2400$
$\bar{\lambda}_{\mathrm{Re}_1}$	21.746 (± 0.003)	27.5005 (± 0.0005)	32.4543 (± 0.0001)	35.6467 (± 0.0002)
$\sqrt{2\sigma_{\mathrm{Re}_1}}$	6.760 (± 0.002)	7.5069 (± 0.0004)	6.4556 (± 0.0001)	5.0249 (± 0.0001)
$\lambda_{\mathrm{ms}}^{\mathrm{Re}_1}$	~ 11	~ 13	~ 15	~ 20

FIG. 4. $\log_{10} P(\lambda)$ obtained from brute-force simulations and $\log_{10} C P_{\text{tail}}(\lambda)$ obtained from Re-control method for several λ_1. The target Reynolds number Re_1 is set to 2100, 2200, 2300, 2400 for (a), (b), (c), (d), respectively. In each panel, we also plot the superexponential fitting curve (15). The parameters Re_0 and λ_0 are set to $\text{Re}_1 - 200$ and $\bar{\lambda}_{\text{Re}_1}$ according to Table I, II. Different lines in the figures correspond to different values of λ_1. To find which lines correspond to which values of λ_1 in the print grayscale version, we note that the value of λ_1 increases as the plateau (for large λ) gets close to zero, as indicated in (a). For the (a)–(c), one can see that, within the range of λ_1 that satisfies the condition of Table I, $P(\lambda)$ agrees with $C P_{\text{tail}}(\lambda)$ for $\lambda < \lambda^*$ [where λ^* is the connecting point between $\log_{10} P(\lambda)$ and $\log_{10} C P_{\text{tail}}(\lambda)$]. This demonstrates the relation (6). For each simulation, we repeat the procedure (i)–(iii) in Sec. II until n_{decay} becomes 3600, except for some lines in (c) and (d): in these cases, because of limited simulation time, we stop the procedure (i)–(iii) before n_{decay} reaches this value. The values of n_{decay} to stop the procedures are summarized in Table III in Appendix C. The statistical errors of each line are small. In order to show this, we divide the obtained data (for each line) into three sets and plot the averaged results over each set in the same figure. Three independent-realization lines are hardly distinguishable, demonstrating small statistical errors. In (d), we only plotted the lines obtained from Re-control method, since the brute-force results are not converged in the tail. ("Fitting" describes the typical part of this unshown brute-force line). With the aid of our Re-control method, the full shape of $P(\lambda)$ can be obtained even in this case, whose tail $C P_{\text{tail}}(\lambda_{\text{decay}})$ corresponds to the inverse of the puff-decaying time scale [as (7)].

More technically, we determine λ^* that minimizes (left-hand side$-$right-hand side)^2 of (16). After determining λ^*, we then calculate C from

$$C = \frac{P_{\text{fit}}(\lambda^*)}{P_{\text{tail}}(\lambda^*)}. \qquad (17)$$

It is straightforward to see if these C and λ^* satisfy (4) and (5).

We plot $C P_{\text{tail}}(\lambda)$ obtained in this way in Fig. 4 for several target Reynolds numbers: $\text{Re}_1 = 2100, 2200, 2300, 2400$. We choose the parameters λ_0, Re_0 following the criteria discussed in the previous section (summarized in Table I together with Table II) for several λ_1. We also plot $P(\lambda)$ obtained from brute-force simulations in the same figure. One can see that $C P_{\text{tail}}(\lambda)$ agrees with $P(\lambda)$ for $\lambda < \lambda^*$ when λ_1 satisfies the criterion.

C. Puff-decaying time scale

In Fig. 5(a), we plot the puff-decaying time scale T_d as a function of λ_1/λ_0, obtained from $C P_{\text{tail}}(\lambda_{\text{decay}})$ by using (7) (where we set $\delta t_m = 1$). We also plot T_d obtained from brute-force simulations. One can see that the estimator of Re-control method agrees with the brute-force result in the range of parameters that satisfy the condition in Table I. We note that our estimator tends to predict larger values than the correct one if the value of λ_1/λ_0 is smaller than this range.

In Fig. 6, we plot the puff-decaying time scale T_d as a function of Re. The results of brute-force and Re-control methods agree with each other for a broad range of Re. We then fit a superexponential function to these data and plot it in the same figure. One can see that the superexponential
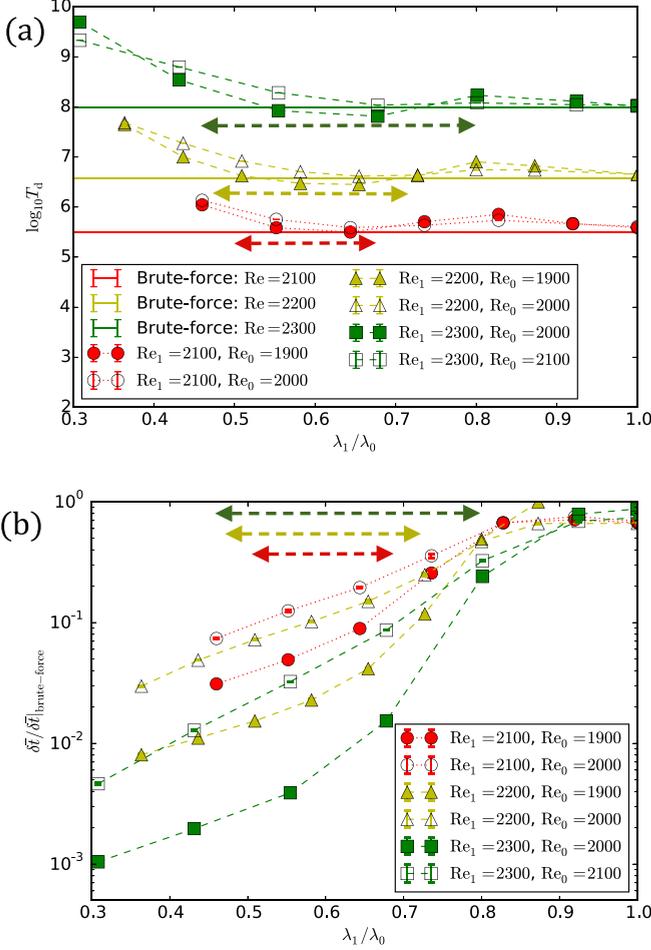
FIG. 5. (a) The logarithm of puff-decaying time scale $\log_{10} T_d$ obtained from Re-control method as a function of the parameter λ_1/λ_0, (where λ_0 is fixed to $\bar{\lambda}_{Re_1}$, whose value is given in Table II). The brute-force estimation of T_d is also shown in the same figure as solid lines. By using dashed double-headed arrows, we indicate the range of λ_1/λ_0 in which the condition of Table I is satisfied. In this range, one can see that the estimators of T_d in brute-force and Re-control methods agree well. (b) The average simulation time $\delta\bar{t}$ to observe one decaying event for Re-control method, divided by the same quantity for the brute-force method $\delta\bar{t}|_{\text{brute-force}}$. How much faster the Re-control method is than the brute-force one is given as the inverse of this quantity. In the range of λ_1 where the condition of Table I is satisfied [indicated by double-headed arrows in the same way as in the (a)], this value takes less than 1, meaning that Re-control method is more efficient than the brute-force method.

curve describes well the obtained numerical data, supporting the existence of superexponential law even for high Reynolds numbers. We expect that the small deviation of data from this superexponential curve at Re = 2500 is an artifact: possible reasons of this deviation are too small value of n_{decay} (Table III in Appendix C) or λ_1 (the description in Appendix D), because of our limited simulation time.

D. Efficiency of Re-control method

Here, we discuss how much the Re-control method accelerates the measurement of the puff-decaying time scale T_d. For this, we consider the time duration of an entire simulation
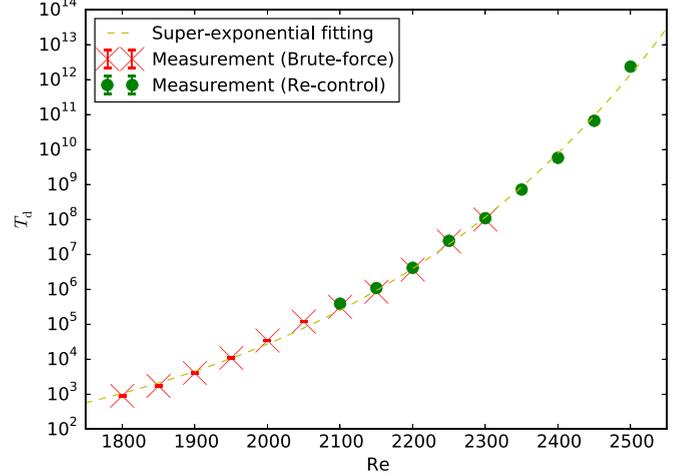
FIG. 6. The puff-decaying time scale T_d obtained from brute-force measurements (from Re = 1800 to 2300 indicated as red crosses) and by Re-control method (from Re = 2100–2500 indicated as green circles). We stop the measurement procedures (i)–(iii) in Sec. II when n_{decay} becomes 3600 for lower Reynolds numbers and much smaller values for higher Reynolds numbers. See Table III in Appendix C for more detail. By dividing the obtained data for each point into three sets, we estimate error bars. These error bars in the figure show small statistical errors. The data points by brute-force measurements (from Re = 1800–2300) and the ones by Re-control method (from Re = 2350–2500) are fitted by a superexponential function defined as $\exp\{\exp[a(\text{Re} - b) + c]\}$ with fitting parameters a,b,c. These parameters are determined using the Levenberg-Marquardt algorithm, which are $a = 2.12 \times 10^{-3}$, $b = 945$, and $c = 0.82$. The obtained superexponential function is plotted as a yellow dashed line in the figure, showing a good agreement with the data points. For Re-control method, we use the parameters $\lambda_0,\lambda_1,\text{Re}_0$ that satisfy the condition in Table I. For more precise values, see Table IV in Appendix D.

to observe one puff-decaying event in average. This time duration includes the preparation of initial conditions in the procedure (i) (Sec. II). We count the total time steps during the repetition of the procedure (i)–(iii), which we denote by T_{all}. Then, the average time duration $\delta\bar{t}$ per unit decaying event is defined as

$$\delta\bar{t} = \frac{T_{\text{all}}}{n_{\text{decay}}}. \tag{18}$$

As this number becomes smaller, one can observe more decaying events in a fixed simulation time, i.e., obtain more statistics to evaluate the time scale of decaying events. We also define the same quantity for brute-force calculations, which we denote by $\delta\bar{t}_{\text{brute-force}}$. In Fig. 5(b), we plot the ratio between these two time durations: $\delta\bar{t}/\delta\bar{t}_{\text{brute-force}}$. One can see that in the range of λ_1 that satisfies the condition of Table I, $\delta\bar{t}/\delta\bar{t}_{\text{brute-force}}$ takes a value from (roughly) 0.005–0.5. Since the inverse of $\delta\bar{t}/\delta\bar{t}_{\text{brute-force}}$ is the speed-up due to the method, we find that the Re-control method is 2–200 times more efficient than the brute-force method. Note that the efficiency of the method increases as λ_1 decreases (or $\text{Re}_1 - \text{Re}_0$ increases). This tendency continues even if the condition in Table I is not satisfied, although, in this case, the systematic errors from the correct result become non-negligible.

V. CONCLUSION

In this paper, in order to measure the puff-decaying time scale efficiently, we introduce a simple procedure where the Reynolds number is controlled during the measurement. The method does not include any complicated procedure: only changing the Reynolds number is required. We thus expect that it can be applied to DNS of Navier-Stokes equation and even to experiments.

The method is applied to the chaotic Barkley model [22], and shows that the superexponential law of the puff-decaying time scale is satisfied even for high Reynolds numbers until Re = 2500, where the puff-decaying time scale is around $10^{12} \sim 10^{13}$ and brute-force calculations cannot be used to estimate it. As a byproduct of the application, we find that the bulk part of $P(\lambda)$ is well described by a superexponential function (see Fig. 2 and Appendix B). Although this fitting function is not necessary for the application of our method, it will be interesting to see if this property holds for even more realistic systems, since the superexponential behavior of a probability function may be the origin of the superexponential time scale of the puff decay [17].

APPENDIX A: BARKLEY MODEL

Here we introduce a coupled map lattice model proposed by Barkley [22] to describe the puff dynamics in pipe flows. This one-dimensional deterministic model consists of only a few hundreds of degrees of freedom, but in spite of the simplified nature of the model, it captures the basic property of puff dynamics, splitting, decaying, and also the superexponential law of the puff-decaying and puff-splitting time scale.

1. Definition of the model

We consider a pipe flow modeled as follows [22]. We denote by $x = 1, 2, \ldots, L$ the axial position of the pipe, and we define, at each position x, the axial velocity of the flows u_x and the turbulence intensity (such as the axial component of the vorticity) q_x. These variables depend on time, which we assume discrete t (= 0, 1, 2, …), i.e., $u^t = (u_x^t)_{x=0}^{L}$ and $q^t = (q_x^t)_{x=0}^{L}$ for $t = 0, 1, 2, \ldots$. We impose periodic boundary conditions to these fields: $u_{L+1}^t = u_1^t$ and $q_{L+1}^t = q_1^t$. For simplicity, we denote by X the set of these two fields: $X = (q, u)$. We set the downstream advection speed to be 1 without loss of generality, which means that q_{x+1}^{t+1} and u_{x+1}^{t+1} are determined from the fields one step before at the position x, q_x^t, u_x^t, and their derivatives (such as $q_x^t - q_{x-1}^t, u_x^t - u_{x-1}^t, q_{x-1}^t - 2q_x^t + q_{x+1}^t, \ldots$). In

laminar flows, the axial velocity field u_x^t takes the largest value 1 (the downstream advection speed) at all the position x. However, in the presence of turbulence, u_x^t becomes inhomogeneous, taking a value less than 1. We take into account this fact in the time-evolution equation of u_x^t by constructing a simple combination of these fields as follows:

$$u_{x+1}^{t+1} = u_x^t + \epsilon_1(1 - u_x^t) - \epsilon_2 u_x^t q_x^t - c(u_x^t - u_{x-1}^t), \quad \text{(A1)}$$

where $\epsilon_1, \epsilon_2, c$ ($\epsilon_1 > 0, \epsilon_2 > 0, c > 0$) are parameters. The second term of this right-hand side enhances the relaminarization of flows, since this second term takes only a positive value, which makes u_{x+1}^{t+1} be closer to the downstream advection speed, while the third term reduces the value of u_{x+1}^{t+1} due to the presence of the turbulence (nonzero value of q_x^t). The fourth term enhances the uniformity of the field u_x^t. When $u_x^t - u_{x-1}^t$ is positive (or negative), it decreases (or increases) u_{x+1}^{t+1} to reduce $u_{x+1}^{t+1} - u_x^{t+1}$ in the next time step.

For the turbulence intensity q_x^t, from the observation that the pipe flow turbulence is locally a chaotic repeller [14], we consider two types of dynamics for q_{x+1}^{t+1}, which are decaying dynamics and chaotic dynamics. When the turbulence intensity is locally smaller than a certain value, the time-evolution equation for the turbulence intensity in that region is a simple diffusion-like equation that enhances relaminarization. However, when it is locally larger than the certain value, the time evolution is described by a chaotic map, introducing a nontrivial nature to this model. Such a threshold value should be a function of u_x^t.
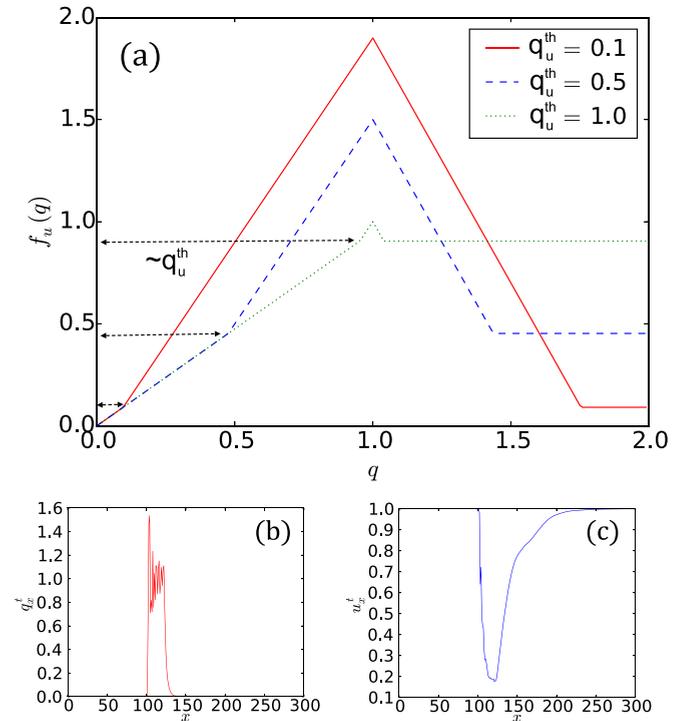

FIG. 7. (a) Functional shape of the tent map $f_u(q)$ for different values of q_u^{th}. As q_u^{th} decreases (or increases), the size of the triangle increases (or decreases), which makes the system to be more (or less) chaotic. We set the Reynolds number Re to 2046, and the rest of the parameters $d, \epsilon_1, \epsilon_2, c, \gamma, \beta$ to 0.15, 0.04, 0.2, 0.45, 0.95, 0.4 according to Ref. [22]. (b), (c) Snapshots of typical configuration of q_x^t (b) and u_x^t (c).

When u_x^t is large (or small), such a threshold value should be small (or large), because large (or small) axial currents easily (or with difficulty) induce turbulence. As the simplest manner, we define this threshold value q_u^{th} as a linear function of u as

$$q_u^{th} \equiv \frac{2000}{2-\gamma}(1 - 0.8\,u)\text{Re}^{-1}, \qquad (A2)$$

where γ is a parameter that takes a value close to 1 (but less than 1), Re is a parameter corresponding to the Reynolds number and u is the local axial velocity, such as u_x^t. The constant $2000/(2-\gamma)$ is merely to adjust the scale of Re to make the transition happen around 2040. By using this threshold value, q_{x+1}^{t+1} is determined as [22]

$$q_{x+1}^{t+1} = F_{u_x^t}\big[q_x^t + d\big(q_{x-1}^t - 2q_x^t + q_{x+1}^t\big)\big], \qquad (A3)$$

where d is a small parameter and $F_u[\cdot]$ is defined from the following map f_u as $F_u[\cdot] \equiv f_u(f_u(\cdot))$:

$$f_u(q) = \gamma q, \qquad (A4)$$

for $q < q_u^{th}$ (decaying dynamics) and

$$f_u(q) = \begin{cases} 2q - q_u^{th}(2-\gamma) & \text{if } q_u^{th} \leqslant q < 1, \\ 4 + \beta - q_u^{th}(2-\gamma) - (2+\beta)q & \text{if } 1 \leqslant q < Q_0, \\ \gamma q_u^{th} & \text{if } Q_0 \leqslant q, \end{cases}$$
$$\qquad (A5)$$

for $q \geqslant q_u^{th}$ (chaotic dynamics) with a constant Q_0 $[\equiv (4 + \beta - q_u^{th}(2-\gamma) - \gamma Q_1)/(2+\beta)]$ and a parameter

β. We note that the chaotic dynamics (A5) is nothing but a tent map. To provide an insight into the map f_u, we show an example of f_u in Fig. 7(a), where one can see that as q_u^{th} becomes larger, the triangle part (the tent-shape part in the figure) becomes smaller, making the system less chaotic. When $q_x^t < q_u^{th}$ [or more precisely $q_x^t + d(q_{x-1}^t - 2q_x^t + q_{x+1}^t) < q_u^{th}$], the time-evolution equation is simply written as $q_{x+1}^{t+1} = \gamma^2[q_x^t + d(q_{x-1}^t - 2q_x^t + q_{x+1}^t)]$. Since we set $\gamma < 1$, one can see that q_x is diffusing with decreasing its intensity by γ^2. We note that, when all q_x ($x = 1, 2, \ldots, L$) follow such dynamics, they converge to 0.

2. Numerical example

We set the parameters $(d, \epsilon_1, \epsilon_2, c, \gamma, \beta)$ to $(0.15, 0.04, 0.2, 0.45, 0.95, 0.4)$ according to Ref. [22]. In the main text, we only change the value of the parameter Re without modifying the others. We start a simulation from a localized configuration, such as the Kronecker-δ configuration with a randomly chosen intensity between 0 and 1. After an initial relaxation time, the puff dynamics becomes statistically stable (especially for Re $\sim$ 2040). In Figs. 7(b), 7(c) we plot snapshots of a puff configuration. Although these dynamics are stable, one can sometimes observe splitting and decaying of puffs in a long-time simulation. The snapshots in Fig. 8 demonstrate such splitting and decaying, observed after simulating the system around 10^5 steps. The duration
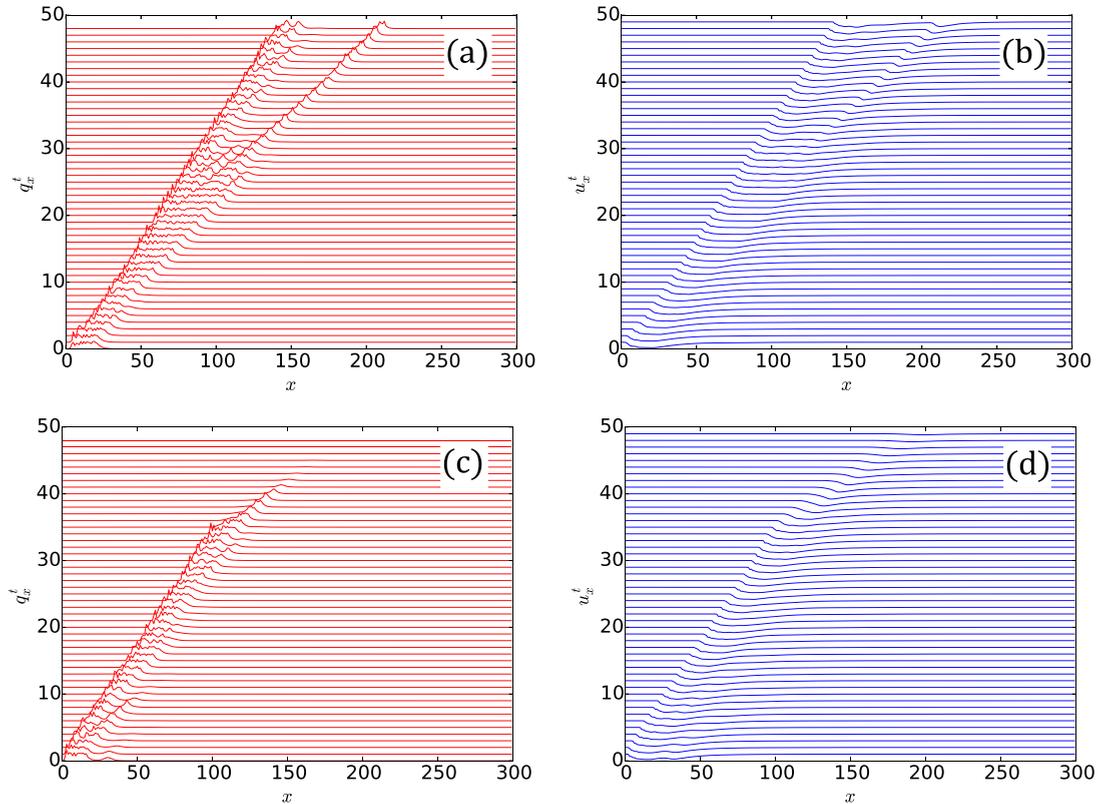

FIG. 8. Snapshots of configurations q [(a) and (c)] and u [(b) and (d)], demonstrating puff splitting [(a) and (b)] and puff decaying [(c) and (d)] for Re $=$ 2046. In each panel, we plot q or u for every five time steps. In order to avoid overlaps of these configurations in a single panel, we shift each configuration along the y axis when time is incremented. More precisely, we plot $q_x^t + (1/5)t$ or $u_x^t + (1/5)t$ for several t ($t = 0, 1, 2, \ldots$) in each panel. We redefine $t = 0$ as the time a few hundred steps before the puff splitting or the puff decaying. The true starting times of these simulations are more than 10^4 steps before this $t = 0$.

of time before the splitting and the decaying is determined stochastically following an exponential law (see Fig. 12 in Ref. [22] for the observation of this law within this model, and also see Refs. [8–12] in more realistic settings).

3. Total turbulence intensity

We define a total turbulence intensity λ as

$$\lambda(X) = \sum_{x=0}^{L} q_x. \qquad (A6)$$

We show a typical time series of $\lambda(X)$ for splitting and decaying in Fig. 1 of the main text. From the figure, we find that $\lambda(X)$ does not take a value less than 1 when there is at least one puff, but it takes less than 1 after the puff decays. We thus define

$$\lambda_{\text{decay}} = 1 \qquad (A7)$$

as a threshold value of the lower bound of $\lambda(X)$, below which the puff completely decays. At the same time, $\lambda(X)$ takes a value around 40 when double puffs occur, and it takes (almost) always a value less than 40 in the presence of a single puff. Since we focus on the dynamics of a single puff and its decaying, we thus define

$$\lambda_{\text{split}} = 41 \qquad (A8)$$

as a threshold value for the upper bound of $\lambda(X)$ [23].

APPENDIX B: SUPEREXPONENTIAL FITTING TO THE PROBABILITY DISTRIBUTION FUNCTION $p(\lambda)$

Here we show a superexponential fitting to the bulk part of the probability distribution function $p(\lambda)$. We consider a probability distribution function $p(\lambda)$ defined as a derivative of the accumulative probability $P(\lambda)$, (8). We show in Fig. 9 numerical examples of $p(\lambda)$ for several Reynolds numbers, together with the derivative of the fitting function (15):

$$p_{\text{fit}}(\lambda) = C \exp\{-\exp[-\tilde{\beta}(\lambda - \tilde{\lambda})] - \tilde{\gamma}(\lambda - \tilde{\lambda})\}, \qquad (B1)$$

where C is a normalization constant, and $\tilde{\beta}, \tilde{\gamma}, \tilde{\lambda}$ are fitting parameters. We note that this fitting function reduces to a Gumbel distribution function [16] when $\tilde{\beta} = \tilde{\gamma}$. Interestingly, as shown in Fig. 9(a), the fitting curve describes perfectly the numerical data in a certain range of λ for several different Reynolds numbers. We also plot the (normalized) fitting parameters, $\tilde{\beta}/\tilde{\beta}(1850), \tilde{\gamma}/\tilde{\gamma}(1850), \tilde{\lambda}/\tilde{\lambda}(1850)$ in Fig. 9(b). The data indicate $\beta \neq \gamma$ in general, namely the distribution function is not described by Gumbel distribution.

To provide an insight into this superexponential form (B1), we introduce an effective Brownian motion describing typical dynamics of $\lambda(X)$. Since it has been observed that the puff-decaying time scale is simply described by a memoryless exponential law [8–12], we assume that the typical dynamics of $\lambda(X)$ itself can be described by the following Brownian process λ_s^t

$$\frac{d\lambda_s^t}{dt} = f(\lambda_s^t) + \xi^t, \qquad (B2)$$

where ξ^t is a Gaussian white noise satisfying zero mean $\langle \xi^t \rangle = 0$ and the delta-function correlation $\langle \xi^t \xi^s \rangle = D\delta(t - s)$ with a noise intensity D. The function $f(\lambda)$ represents the
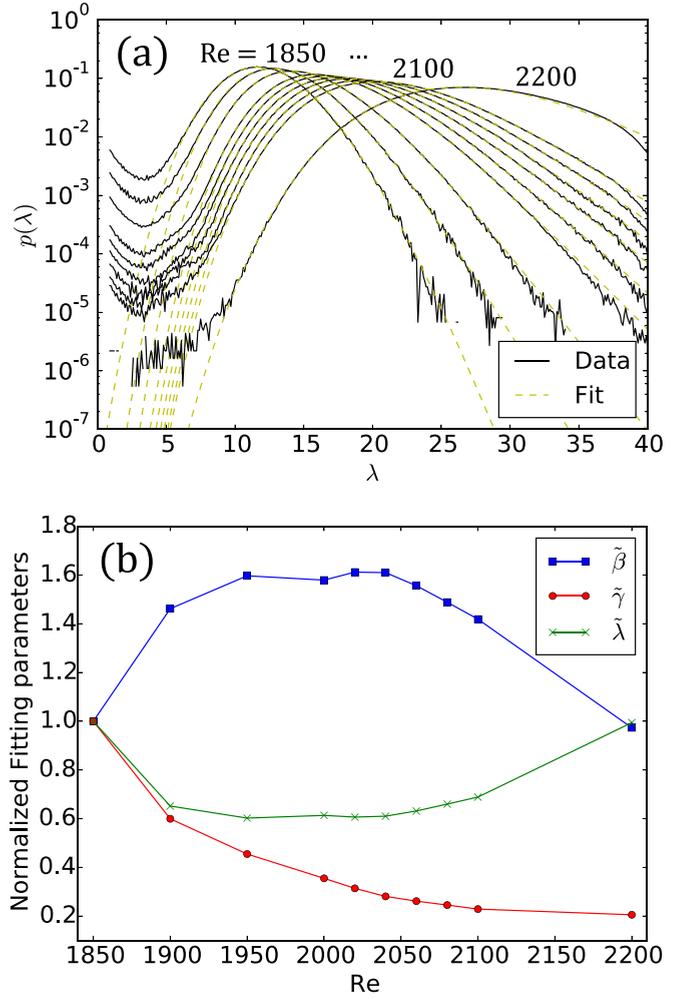

FIG. 9. (a) The probability distribution functions of λ, $p(\lambda)$ for several values of the Reynolds number Re (Re = 1850, 1900, 1950, 2000, 2020, 2040, 2060, 2080, 2100, 2200), which are measured from brute-force simulations. We also plot the superexponential curve (B1) by using the parameters determined by fitting to the data. The agreement between the fitting curve and the numerical data is excellent for a certain range of λ. (b) The (normalized) fitting parameters, $\tilde{\beta}/\tilde{\beta}(1850), \tilde{\gamma}/\tilde{\gamma}(1850), \tilde{\lambda}/\tilde{\lambda}(1850)$ as a function of the Reynolds number, where the values of $\tilde{\beta}(1850), \tilde{\gamma}(1850), \tilde{\lambda}(1850)$ are 0.1012, 1.574, 38.75, respectively. One can see that $\tilde{\beta}$ and $\tilde{\lambda}$ show a plateau in the range from Re = 1950 to Re = 2050, whereas $\tilde{\gamma}$ is monotonically decreasing.

effective force describing the dynamics of the turbulence intensity. For this function, we consider two contributions, $f_-(\lambda)$ and $f_+(\lambda)$. The first contribution is to reduce the size of the puff at the interface between the turbulent region and the Laminar region. This contribution does not depend on the value of λ, so that we model this effect as a constant term f_0, i.e., $f_-(\lambda) = -f_0$. The second contribution is to enlarge the turbulent region. When the turbulence intensity is small, puffs immediately develop their intensity, whereas when the turbulence intensity is large, the dynamics immediately lose such a driving force. To model this behavior, we assume that $f_+(\lambda)$ is written as an exponential function $f_+(\lambda) = \alpha e^{-\beta(\lambda - \lambda_0)}$ with three parameters α, β, and λ_0. To sum up f_+ and f_-, we

TABLE III. $n_{\mathrm{decay}}^{\max}$: the values of n_{decay} when we stop the measurement procedures (i)–(iii) in Sec. II. For Re-control method, $n_{\mathrm{decay}}^{\max}$ for λ_1 and Re_0 specified in Table IV is shown.

Re_1	Brute-force	Re-control
1800	3600	–
1850	3600	–
1900	3600	–
1950	3600	–
2000	3600	–
2050	3600	–
2100	3600	3600
2150	3600	3600
2200	3600	3600
2250	2746	3600
2300	578	3600
2350	–	1647
2400	–	151
2450	–	149
2500	–	12

get $f(\lambda) = -f_0 + \alpha e^{-\beta(\lambda - \lambda_0)}$. Since the stationary distribution function of λ_s^t, $p_{\mathrm{st}}(\lambda)$, is derived as the canonical distribution function $e^{(1/D) \int d\lambda f(\lambda)}$, we thus obtain

$$p_{\mathrm{st}}(\lambda) = \tilde{C} \exp \left\{ -\frac{f_0}{D}\lambda - \frac{\alpha}{D\beta} \exp\left[-\beta(\lambda - \lambda_0) \right] \right\} \quad \text{(B3)}$$

with a normalization constant $\tilde{C}$. By redefining the parameters in this expression, one can see that $p_{\mathrm{st}}(\lambda)$ is equivalent to the fitting function (B1).

APPENDIX C: VALUES OF n_{decay} WHEN STOPPING THE MEASUREMENTS

For getting the data in Figs. 4, 5, 6, we stop the measurement procedure (i)–(iii) in Sec. II when n_{decay} reaches a certain

TABLE IV. The values of $\lambda_0, \lambda_1, \mathrm{Re}_0$ used in Fig. 6 for Re-control method.

Re_1	$\lambda_0 (= \bar{\lambda}_{\mathrm{Re}_1})$	λ_1	$\mathrm{Re}_1 - \mathrm{Re}_0$
2100	21.75	14	200
2150	24.55	16	200
2200	27.50	18	200
2250	30.23	18	200
2300	32.45	22	200
2350	34.22	22	200
2400	35.65	24	200
2450	36.81	24	300
2500	37.73	24	300

value, which we denote by $n_{\mathrm{decay}}^{\max}$. We summarize $n_{\mathrm{decay}}^{\max}$ in Table III.

APPENDIX D: VALUES OF PARAMETERS $\lambda_0, \lambda_1, \mathrm{Re}_0$ FOR FIG. 6

In Table IV, we summarize the parameters used in Fig. 6 for Re-control method. These parameters are chosen according to the condition in Table I.

For $\mathrm{Re} = 2500$, in order to observe the puff-decaying event in our limited simulation time, we needed to set λ_1 to be close enough to $\lambda_{\mathrm{ms}}^{\mathrm{Re}_1}$. This is a possible reason why the predicted value of puff-decaying time scale for $\mathrm{Re} = 2500$ in Fig. 6 is slightly higher than the superexponential curve, because as seen from Fig. 5(a), as λ_1 gets close to $\lambda_{\mathrm{ms}}^{\mathrm{Re}_1}$, the method becomes much faster, but the estimated value of T_d tends to be larger than the correct value.

[1] O. Reynolds, An experimental investigation of the circumstances which determine whether the motion of water shall be direct or sinuous, and of the law of resistance in parallel channels, Proc. R. Soc. London **35**, 84 (1883).

[2] A. G. Darbyshire and T. Mullin, Transition to turbulence in constant-mass-flux pipe flow, J. Fluid Mech. **289**, 83 (1995).

[3] H. Faisst and B. Eckhardt, Sensitive dependence on initial conditions in transition to turbulence in pipe flow, J. Fluid Mech. **504**, 343 (2004).

[4] B. Eckhardt, Introduction. Turbulence transition in pipe flow: 125th anniversary of the publication of Reynolds' paper, Philos. Trans. R. Soc. London A **367**, 449 (2009).

[5] I. J. Wygnanski and F. H. Champagne, On transition in a pipe. Part 1. The origin of puffs and slugs and the flow in a turbulent slug, J. Fluid Mech. **59**, 281 (1973).

[6] J. Peixinho and T. Mullin, Decay of Turbulence in Pipe Flow, Phys. Rev. Lett. **96**, 094501 (2006).

[7] A. P. Willis and R. R. Kerswell, Critical Behavior in the Relaminarization of Localized Turbulence in Pipe Flow, Phys. Rev. Lett. **98**, 014501 (2007).

[8] B. Hof, J. Westerweel, T. M. Schneider, and B. Eckhardt, Finite lifetime of turbulence in shear flows, Nature (London) **443**, 59 (2006).

[9] B. Hof, A. de Lozar, D. J. Kuik, and J. Westerweel, Repeller or Attractor? Selecting the Dynamical Model for the Onset of Turbulence in Pipe Flow, Phys. Rev. Lett. **101**, 214501 (2008).

[10] A. de Lozar and B. Hof, An experimental study of the decay of turbulent puffs in pipe flow, Philos. Trans. R. Soc. London A **367**, 589 (2009).

[11] M. Avila, A. P. Willis, and B. Hof, On the transient nature of localized pipe flow turbulence, J. Fluid Mech. **646**, 127 (2010).

[12] D. J. Kuik, C. Poelma, and J. Westerweel, Quantitative measurement of the lifetime of localized turbulence in pipe flow, J. Fluid Mech. **645**, 529 (2010).

[13] K. Avila, D. Moxey, A. de Lozar, M. Avila, D. Barkley, and B. Hof, The onset of turbulence in pipe flow, Science **333**, 192 (2011).

[14] B. Eckhardt, T. M. Schneider, B. Hof, and J. Westerweel, Turbulence transition in pipe flow, Annu. Rev. Fluid Mech. **39**, 447 (2007).

[15] R. A. Fisher and L. H. C. Tippett, Limiting forms of the frequency distribution of the largest or smallest member of a sample, in *Mathematical Proceedings of the Cambridge Philosophical Society* (Cambridge University Press, Cambridge, 1928), Vol. 24, p. 180.

[16] E. J. Gumbel, Les valeurs extrêmes des distributions statistiques, Ann. Inst. Henri Poincaré **5**, 115 (1935).

[17] N. Goldenfeld, N. Guttenberg, and G. Gioia, Extreme fluctuations and the finite lifetime of the turbulent state, Phys. Rev. E **81**, 035304 (2010).

[18] N. Goldenfeld and H.-Y. Shih, Turbulence as a Problem in Nonequilibrium statistical mechanics, J. Stat. Phys. **167**, 575 (2017).

[19] M. Sipos and N. Goldenfeld, Directed percolation describes lifetime and growth of turbulent puffs and slugs, Phys. Rev. E **84**, 035304 (2011).

[20] H.-Y. Shih, T.-L. Hsieh, and N. Goldenfeld, Ecological collapse and the emergence of traveling waves at the onset of shear turbulence, Nature Phys. **12**, 245 (2016).

[21] H. Chaté and P. Manneville, Spatio-temporal intermittency in coupled map lattices, Physica D **32**, 409 (1988).

[22] D. Barkley, Simplifying the complexity of pipe flow, Phys. Rev. E **84**, 016309 (2011).

[23] We observed that the condition for λ_{decay} is satisfied with $\lambda_{\text{decay}} = 1$ for all the Reynolds numbers used in this paper, i.e., once $\lambda < \lambda_{\text{decay}}$ the puff always decays afterward. For λ_{split}, we also observed that the puff prefers to be in a double (or a single) puff state for $\lambda > \lambda_{\text{split}}$ (or $\lambda < \lambda_{\text{split}}$) with $\lambda_{\text{split}} = 41$ for most of the Reynolds numbers (Re $\leqslant$ 2300). For higher Reynolds numbers (Re $\geqslant$ 2400), there is a precursor of slug states, where a single puff extends in the space. In these cases, the puff is often single when $\lambda > \lambda_{\text{split}}(= 41)$ is observed, and then split into two or more without changing the total turbulence intensity. We did not take into account these effects, by keeping $\lambda_{\text{split}} = 41$ (and reinitializing the state when the puff extends in the space). To properly define a single-puff state in higher Reynolds numbers is an important open problem.